EFFECTS OF SCREENING ON THE TWO-DIMENSIONAL ELECTRON TRANSPORT PROPERTIES IN MODULATION DOPED HETEROSTRUCTURES

O. SEN[1], C. BESIKCI[1] and B. TANATAR[2]

[1]Electrical Engineering Department, Middle East Technical University, 06531 Ankara, Turkey
[2]Physics Department, Bilkent University, 06533 Ankara, Turkey

Abstract—The effects of screening on the polar optical phonon scattering rates and on the transport properties of the two-dimensional electron gas in AlGaAs/GaAs modulation doped heterostructures have been investigated through Monte Carlo simulations incorporating the three valleys of the conduction band, size quantization in the Γ valley and the lowest three subbands in the quantum-well. At typical sheet densities observed in modulation doped field-effect transistors, screening considerably affects the electron transport properties under moderately large fields and at low temperatures, by lowering the intrasubband polar-optical phonon scattering rates especially in the first subband. The results show that screening, which is usually ignored in device Monte Carlo simulations, should be included in the simulation in order to be able to predict the device performance correctly. © 1998 Elsevier Science Ltd. All rights reserved

1. INTRODUCTION

Electronic systems in confined semiconductor structures are under intense study[1,2] for quite some time. With the recent developments in the III–V semiconductor technology, III–V heterostructures have successfully been used to build high-performance electron devices such as modulation doped field-effect transistors (MODFETs) and optical devices such as quantum-well photodetectors and lasers. Due to the superior transport properties of the two-dimensional (2D) electron gas, MODFETs have been a promising device for high-performance microwave and digital applications. In order to understand the device physics, optimize the device performance and use the desirable transport properties of the 2D electron gas efficiently, various models have been developed to simulate these devices[3–11]. The Monte Carlo technique, the most powerful and complete method in device analysis, has widely been used in the simulation and optimization of MODFETs[9–11]. While the most important scattering mechanisms such as polar optical phonon and acoustic phonon scattering have been included in these simulations, some mechanisms which are assumed to be of the second order, such as screening, have usually been ignored. In this paper, we investigate the effects of screening on 2D polar optical phonon scattering rates and on the transport properties of the 2D electron gas in modulation doped heterostructures through Monte Carlo simulations. We ignore the effects of screening on the acoustic phonon scattering as justified by the previous reports[12–15].

In Section 2 formulation of the 2D polar-optical phonon scattering rates, including the screening effects, is presented. The Monte Carlo simulation procedure is given in Section 3. Section 4 presents the simulation results and discussion. The conclusion is given in Section 5.

2. POLAR OPTICAL PHONON SCATTERING RATES

We consider a single-well heterostructure in a three-subband model. Based on a variational approach[16,17], the subband wavefunctions are approximated as

$$\phi_1(z) = (b^3/2)^{1/2} z \exp(-bz/2) \tag{1}$$

$$\phi_2(z) = (3b^3/2)^{1/2} z(1 - bz/3)\exp(-bz/2) \tag{2}$$

$$\phi_3(z) = (3b^3)^{1/2} z(1 - 2bz/3 + b^2z^2/12)\exp(-bz/2) \tag{3}$$

where the parameter $b = (33m^*e^2N_s/\varepsilon_0)^{1/3}$, is related to the sheet electron density, N_s. The polar-optical phonon scattering rates are calculated using Fermi's golden rule[18,19],

$$\Gamma_{ij}(k) = \frac{e^2 w_{LO}}{2}\left(n_B(w_{LO}) + \frac{1}{2} \pm \frac{1}{2}\right)$$
$$\times \int d^2q \frac{H_{jiij}^{\text{eff}}(q)}{q}\delta(E_i(k) \mp w_{LO} - E_j(k \mp q)) \tag{4}$$

where the upper and lower signs refer to the emission and absorption processes, respectively. $n_B(w_{LO})$ is the Bose distribution function which gives the average number of phonons with energy w_{LO} at temperature T. Screening effects are taken into account within a static approximation by considering an effective interaction H^{eff} defined in terms of the dielectric matrix[19]

$$H_{ijkl}(q) = \sum_{mn} \varepsilon_{ijnm}(q, w = 0) H^{eff}_{mnkl}(q) \qquad (5)$$

The subband form factors in the absence of screening are expressed by

$$H_{ijkl}(q) = \int_0^\infty dz \int_0^\infty dz' e^{-q|z-z'|} \phi_i(z')\phi_j(z')\phi_k(z)\phi_l(z) \qquad (6)$$

in which the variational wave functions are used. The dielectric matrix embodying the screening effects is given in the random phase approximation (RPA) by

$$\varepsilon_{ijnm}(q) = \delta_{im}\delta_{jn} - V_{ijnm}(q)\chi_{nm}(q) \qquad (7)$$

where $\chi_{nm}(q)$ is the static polarizability. The form factors and the Coulomb interaction matrix elements are related by $H_{ijkl}(q) = V_{ijkl}(q)/(2\pi e^2/q)$. In this work, we consider only the static dielectric function. The dynamical effects[19] worthy of a separate study are beyond the scope of the present calculation. The usual Thomas–Fermi screening corresponds to the $q \rightarrow 0$ limit of our dielectric function. The static screening approximation adopted here should be appropriate for large carrier densities, since $\hbar w_{LO}$ remains small compared with the characteristic energy (i.e. plasmon energy) of the electron gas.

The subband energies for $N_s = 10^{11}$, 5×10^{11} and 10^{12} cm^{-2} at $T = 77$ and 300 K are taken from the self-consistent calculations of Yokoyama and Hess[20,21] and Stern and Das Sarma[22]. The matrix elements of the static dielectric function $\varepsilon(q)$ are calculated by keeping the full temperature dependence. Figure 1 shows the polar-optical phonon scattering rates at $T = 77$ K and $N_s = 10^{12}$ cm^{-2}. We observe that the screening effects are appreciable only for intra-subband rates (for both emission and absorption), whereas the inter-subband rates show almost no dependence on the dielectric screening. This is mainly due to the rapidly decreasing strength of the intersubband Coulomb matrix elements $H_{ijkl}(q)$. We have also found that screening effects almost diminish for densities $N_s \leq 5 \times 10^{11}$ cm^{-2}, at room temperature.

3. MONTE CARLO SIMULATIONS

In order to investigate the effects of screening on the transport properties of the 2D electron gas, steady-state and transient Monte Carlo simulations

have been performed for the Al$_{0.3}$Ga$_{0.7}$As/GaAs quantum well. The simulations have been carried out for both screened and unscreened cases at three different 2D electron densities ($N_s = 10^{11}$, 5×10^{11} and 10^{12} cm^{-2}) and at temperatures of 77 and 300 K. Three valleys of the conduction band (Γ, L and X) and band nonparabolicities have been included by considering size quantization in the Γ valley and the first three subbands in the quantum-well. L and X valleys have been assumed to have 3D properties. We have also treated the electrons with energies larger than the third subband energy as three-dimensional. This assumption can be justi-
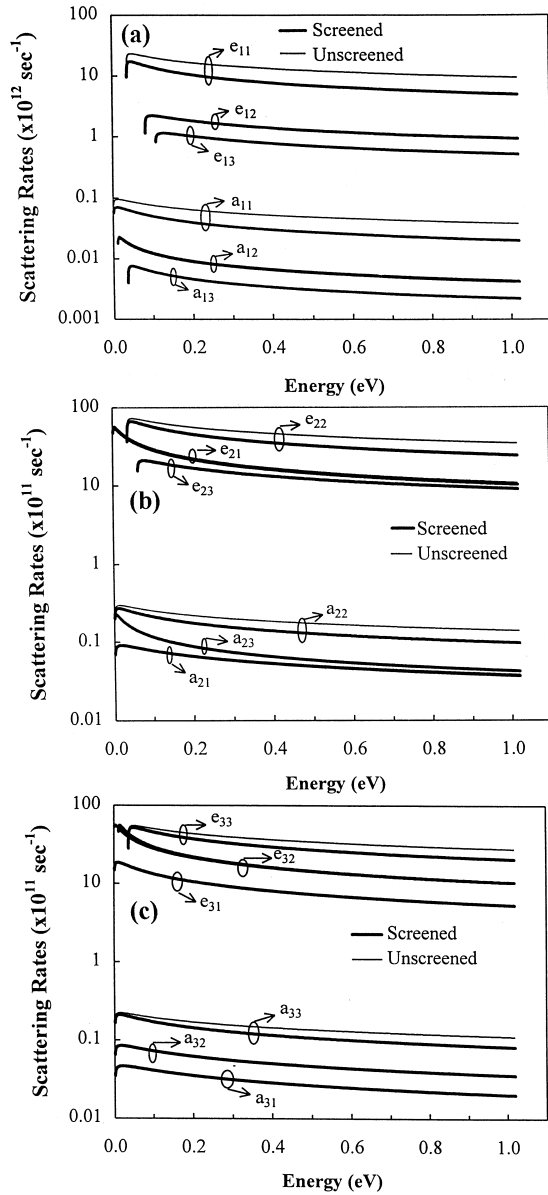

Fig. 1. The intra and intersubband, screened and unscreened polar-optical phonon scattering rates as a function of energy at $N_s = 10^{12}$ cm^{-2} and $T = 77$ K for (a) subband-1, (b) subband-2 and (c) subband-3

fied due to the closer spacing of the energy levels at high energies which forms a quasicontinuum like the case in the bulk material. The simulation starts by launching the electron in the two-dimensional system. The trajectory of the electron subjected to two-dimensional scattering mechanisms is followed under the applied field and the electron is placed in the 3D system after it is scattered to the third subband or to the L and X valleys. After the electron enters the 3D system, it is subjected to 3D scattering mechanisms until it is scattered back to the 2D system. A similar way of two to three dimensional coupling was used by Park and Brennan[11] in their Monte Carlo simulations. However, their approach ignores the third and higher subbands and places the electron in the 3D system after the electron's energy exceeds the band bending energy. We have observed that including the third subband in describing the intersubband scattering processes yields much more accurate results. The scattering mechanisms included in the simulation are polar optical phonon scattering, acoustic phonon scattering and intervalley (equivalent and nonequivalent) scattering. We have neglected the impurity scattering effects which may come from background or remote impurities. The 3D scattering rates used are the same as those given by Fawcett et al.[23].

4. RESULTS AND DISCUSSION

Band occupancy vs electric field at $N_s = 10^{12}$ cm^{-2} and $T = 77$ K is shown in Fig. 2. The curves labeled 3D-Γ refer to the unquantized electrons in the Γ-valley (electrons with energies larger than the third subband energy). As mentioned before, L and X valleys of the conduction band have been assumed to have 3D-like properties. In the field range of 0–20 kV/cm, the fraction of the electron population residing in the quantized system is significant which indicates the necessity of taking size quantization into account for an accurate description of carrier transport in quantum well devices. The results presented in Fig. 2(b) indicate that the electron population in the 3D-Γ valley is less than 10% throughout the entire field range for both screened and unscreened cases. This shows that significant intervalley transfer to the L valley starts once the electron energy in the quantized system is large enough to populate the third subband. Based on these results, it can be concluded that taking only the lowest two subbands into account and treating the electron as a three-dimensional electron after it is scattered to the third subband is a reasonable approximation in the Monte Carlo analysis of GaAs based quantum well devices. Above 20 kV/cm, the populations of both L and X valleys become considerably high and both valleys must be considered for proper description of transport. In most of the previous work on device analysis, the X valley of the conduction band was ignored. At this

2D electron density and temperature, significant differences between the band populations in screened and unscreened cases are seen in the field range of 0–20 kV/cm, where the quantized electron population is considerably high. While the population of subband-1 in the screened case is lower, the effects of screening increase the occupancy of subband-2 under moderately large field strengths. This may be attributed to the decrease in intrasubband polar-optical phonon emission rate of 2D electrons in subband-1 by screening. In the screened case, the electron energy in the first subband increases more rapidly with increasing field strength which results in a faster transfer to subband-2 and to upper lying valleys and a lower subband-1 population. The intrasubband polar-optical phonon scattering rates of subband-2 also decrease with screening. However, screening increases the population of this subband due to a faster transfer of subband-1 electrons to this subband. Similarly, the increase of the L valley population by screening is due to a more rapid transfer of 2D electrons in subband-1 and subband-2 to this valley.

Figure 3(a) shows the overall electron velocity and energy (averaged over the electrons in subband-1, subband-2, 3D-Γ, L and X valleys) at $N_s = 10^{12}$ cm^{-2} and $T = 77$ K. In the screened case, the critical field is shifted to lower fields due to more rapid electron transfer to the higher effective

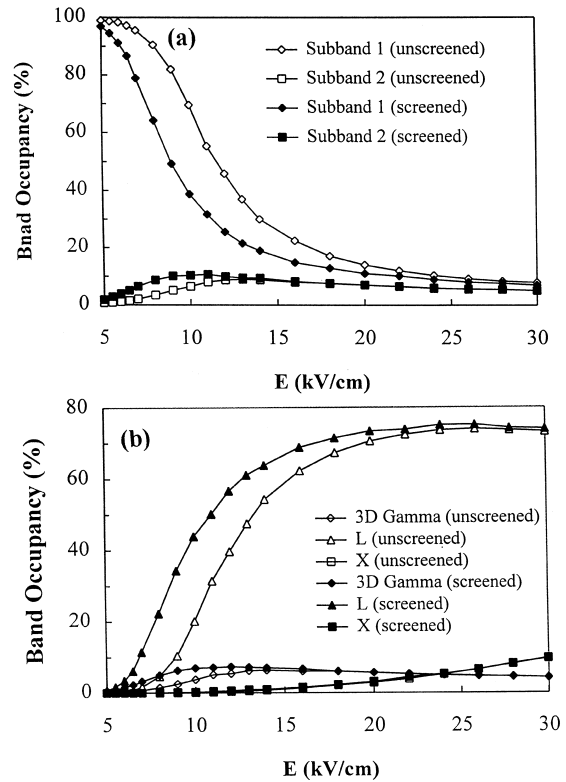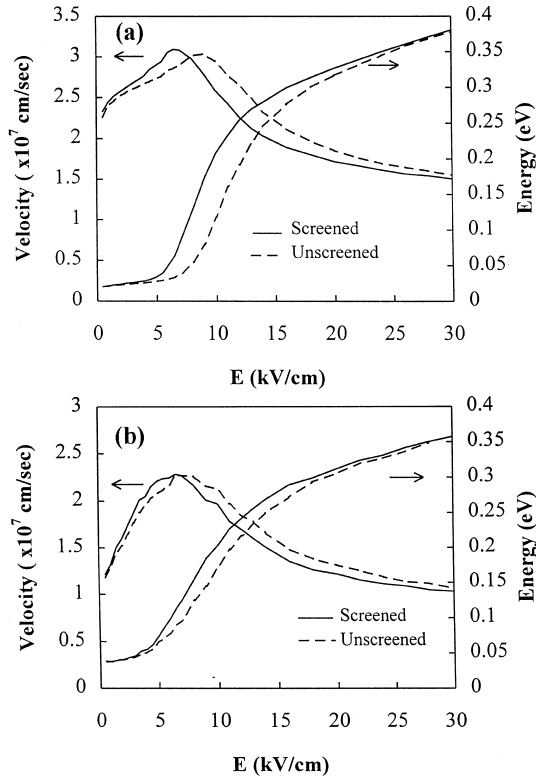Fig. 2. The band occupancies as a function of the applied field at $N_s = 10^{12}$ cm^{-2} and $T = 77$ K

Fig. 3. (a) The steady-state electron velocity and average energy as a function of the applied field at $N_s = 10^{12}$ cm^{-2} and $T = 77$ K. (b) Same as (a) at $T = 300$ K. Velocity and energy are averaged over the electrons in the subbands, 3D-Γ, L and X valleys

mass satellite valleys. This can be attributed to the decrease in the intrasubband polar-optical phonon emission rates and relatively rapid increase of energy in the subbands. In this case, the overall energy is larger due to the higher electron energies in the subbands. As can be seen in Fig. 3(a), at this 2D electron density and temperature, if the screening effects are turned off, an error of 30% in the overall electron energy and an error of 20% in the overall velocity would be introduced under moderately large field strengths.

Figure 3(b) displays the results of the simulations performed at $N_s = 10^{12}$ cm^{-2} and $T = 300$ K. At this temperature, the effects of screening on the transport properties are less significant. Simulations carried out at a 2D electron density of $N_s = 10^{11}$ cm^{-2} resulted in insignificant differences between the screened and unscreened cases both at $T = 77$ and 300 K. At $N_s = 5 \times 10^{11}$ cm^{-2}, the maximum error introduced in the estimation of the overall velocity by ignoring screening effects was around 10% at $T = 77$ K and under moderately large field strengths. $T = 300$ K simulations have shown that the effects of screening on the transport properties are negligible at this 2D density.

In order to investigate the effects of screening on the nonstationary transport characteristics of the

2D electron gas, we have also carried out transient ensemble Monte Carlo simulations under rapidly varying electric fields. Figure 4 shows the transient band occupancy, electron velocity and energy under an electric field stepped from 3 to 10 kV/cm. In Fig. 4(a), the curve labeled 3D system refers to the sum of the occupancies of the 3D-Γ, L and X valleys. In Fig. 4(b), velocity and energy are averaged over the electrons in the subbands, 3D-Γ, L and X valleys. Figure 5 displays the electron velocity and energy under a ramping field. Under both field profiles, the peak velocity and energy are considerably underestimated if the screening is ignored. In the screened case, velocity increases more rapidly and the peak value is higher due to the lower intrasubband scattering rates. However, in this case, transfer of electrons to the upper valleys takes place and steady-state is reached sooner due to the higher rate of increase of energy in the subbands. The larger velocity overshoot in the screened case is due to the
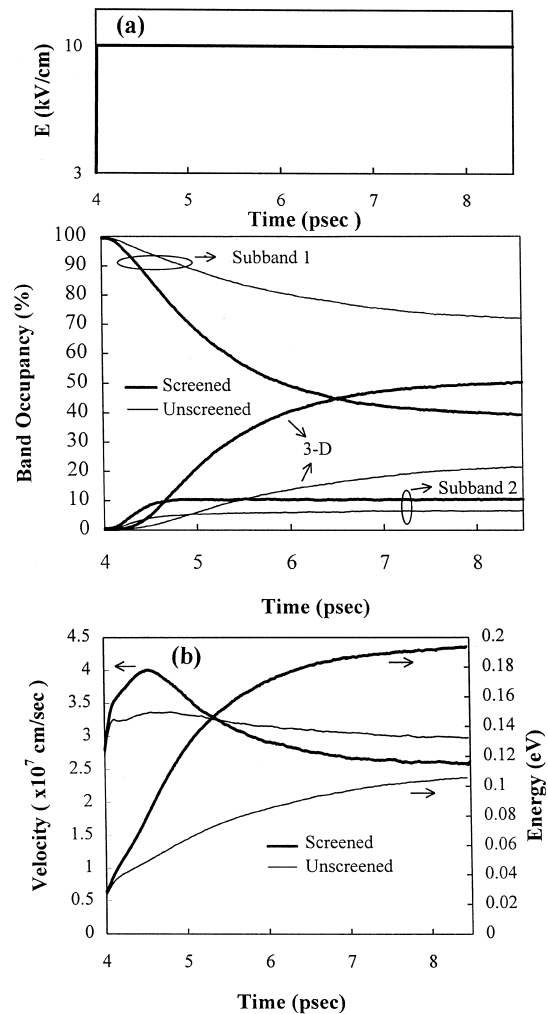

Fig. 4. (a) The transient band-occupancy under a step-field. Curves labeled 3D refer to a sum over the 3D-Γ, L and X valleys. (b) Transient average velocity and energy
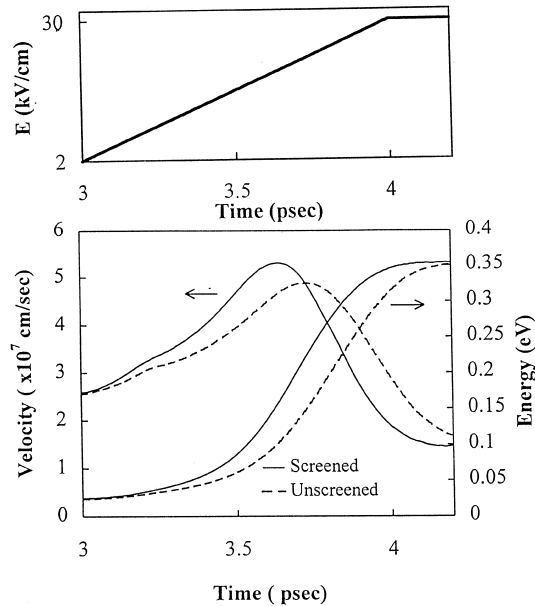
Fig. 5. The transient velocity and energy under a strong ramping field

larger low-field mobility resulting from lower polar-optical phonon scattering rates.

5. CONCLUSION

The results presented above clearly show that screening is an important factor that needs to be taken into account in low-temperature Monte Carlo simulations of quantum-well devices such as MODFETs. The reduction in the intra-subband polar-optical phonon scattering rates due to screening significantly affects both the steady-state and transient transport properties of the heterostructure under moderately large field strengths. While the effects of screening diminish for densities $N_s \leq 5 \times 10^{11}$ cm^{-2}, its effects become significant around $N_s = 10^{12}$ cm^{-2}. Since modulation doped heterostructures with 2D electron densities larger than this value can be produced by the present III–V technology, the effects of screening on the transport properties and on the device characteristics will be even more serious in these heterostructures.

Therefore, the effects of screening on polar-optical phonon scattering should be taken into account in the analysis of these devices.

REFERENCES

1. Ando, T., Fowler, A. B. and Stern, F., *Rev. Mod. Phys.*, 1982, **54**, 437.
2. Weisbuch, C. and Vinter, B., *Quantum Semiconductor Structures*. Academic Press, New York, 1991.
3. Drummond, T. J., Morkoc, H., Lee, K. and Shur, M., *IEEE Electron Dev. Lett.*, 1982, **3**, 338.
4. Park, K. and Kwack, K. D., *IEEE Trans. Electron Dev.*, 1986, **33**, 673.
5. Wang, G. W. and Ku, W. H., *IEEE Trans. Electron Dev.*, 1986, **33**, 657.
6. Widiger, D., Kizilyalli, I. C., Hess, K. and Coleman, J. J., *IEEE Trans. Electron Dev.*, 1985, **32**, 1092.
7. Tang, J. Y. F., *IEEE Trans. Electron Dev.*, 1985, **32**, 1817.
8. Yoshida, J. and Kurata, M., *IEEE Electron Dev. Lett.*, 1984, **5**, 508.
9. Tomizawa, K. and Hashizume, N., *IEEE Trans. Electron Dev.*, 1988, **35**, 849.
10. Ravaioli, U. and Ferry, D. K., *IEEE Trans. Electron Dev.*, 1986, **33**, 677.
11. Park, D. H. and Brennan, K. F., *IEEE Trans. Electron Dev.*, 1989, **36**, 1254.
12. Price, P. J., *Ann. Phys. N. Y.*, 1981, **133**, 217.
13. Price, P. J., *Surf. Sci.*, 1982, **113**, 199.
14. Price, P.J., *Surf. Sci.*, 1984, **143**, 145.
15. Walukiewicz, W., *Phys. Rev. B*, 1988, **37**, 8530.
16. Stern, F. and Howard, W. E., *Phys. Rev.*, 1967, **163**, 816.
17. Mori, S. and Ando, T., *Phys. Rev.*, 1979, **19**, 6433.
18. Ridley, B. K., *J. Phys. C*, 1982, **15**, 5899.
19. Sotirelis, P., von Allmen, P. and Hess, K., *Phys. Rev. B*, 1993, **47**, 12744.
20. Yokoyama, K. and Hess, K., *Phys. Rev. B*, 1985, **31**, 6872.
21. Yokoyama, K. and Hess, K., *Phys. Rev. B*, 1986, **33**, 5595.
22. Stern, F. and Das Sarma, S., *Phys. Rev. B*, 1984, **30**, 840.
23. Fawcett, W., Boardman, A. D. and Swain, S., *J. Phys. Chem. Solids*, 1970, **31**, 1963.